Giant off-resonance resistance spike related phenomena in irradiated ultraclean two-dimensional electron systems.

J. Iñarrea
Escuela Politécnica Superior, Universidad Carlos III, Leganes, Madrid, 28911, Spain

(Dated: February 25, 2013)

We report on theoretical studies of a recently discovered strong radiation-induced magnetoresistance spike obtained in ultraclean two-dimensional electron systems at low temperatures. The most striking feature of this spike is that it shows up on the second harmonic of the cyclotron resonance and with an amplitude that can reach an order of magnitude larger than the radiation-induced resistance oscillations. We apply the radiation-driven electron orbits model in the ultraclean scenario. Accordingly, we calculate the elastic scattering rate (charged impurity) which will define the unexpected resonance spike position. We also obtain the inelastic scattering rate (phonon damping), that will be responsible of the large spike amplitude. We present a microscopical model to explain the dependence of the Landau level width on the magnetic field for ultraclean samples. We find that this dependence explains the experimental shift of the resistance oscillations with respect to the magnetic field found in this kind of samples. We study also recent results on the influence of an in-plane magnetic field on the spike. We are able to reconcile the obtained different experimental response of both spike and resistance oscillations versus an increasing in-plane field. The same model on the variation of the LL width, allows us to explain such surprising results based in the increasing disorder in the sample caused by the in-planed magnetic field. Calculated results are in good agreement with experiments. These results would be of special interest in nanophotonics; they could lead to the design of novel ultrasensitive microwave detectors.

PACS numbers:

I. INTRODUCTION

Quantum Hall effect and radiation-matter coupling[1] are two of the most remarkable topics in Condensed Matter Physics. Accordingly, transport excited by radiation in a two-dimensional electron system (2DES) has been always a central topic in basic and applied research. In the last decade it was discovered that when a 2DES in a perpendicular magnetic field (B) is irradiated, mainly with microwaves (MW), some striking effects are revealed: radiation-induced magnetoresistance (R_{xx}) oscillations and zero resistance states (ZRS)[2,3]. These remarkable effects show up at low B and high mobility samples. It is important to achieve a complete understanding of the physical mechanisms being responsible of them and not only for the basic knowledge purpose but also for the potential applications in nanoelectronics. Different theories have been proposed to explain these effects[4–12] but the physical origin is still being questioned. In the same way, a great effort has also been made from the experimental side[13–20]. Of course the obtained experimental results always mean a real challenge for the existent theoretical models. Therefore, a comparison of experiment with theory could help to identify the importance of the different approaches in these theories. Thus, as an example, it has been recently published experimental results on the dependence of the oscillations with radiation power[21,22] where a very solid result has been obtained in terms of a sublinear relation, similar to a square root. Yet, some theories predicted a linear dependence[23] between R_{xx} oscillations and radiation power.

One of the most interesting and challenging experimental result, recently obtained[24,25] and as intriguing as ZRS, consists in a strong resistance spike which shows up far off-resonance. It occurs at twice the cyclotron frequency, $w \approx 2w_c$[24,25], were w is the radiation frequency and w_c the cyclotron frequency. The amplitude of such a spike is very large reaching an order of magnitude regarding the radiation-induced R_{xx} oscillations. In the same experiments it is also reported the behavior of the resistance spike with different radiation frequencies, temperature (T) and radiation power (P). Remarkably, the only different feature in these experiments[24,25] is the use of ultraclean samples with mobility $\mu \sim 3 \times 10^7 cm^2/Vs$ and lower temperatures, $T \sim 0.4K$. Yet, for the previous, "*standard*", experiments[2,3] the mobility is lower, ($\mu < 10^7 cm^2/Vs$) and T higher, ($T \geq 1.0K$). Much more recently experimental results on this off-resonance giant resistance spike have been presented by the same authors[26]. This time they add an in-plane magnetic field to the standard experimental set-up. Remarkably, they obtain that the radiation-induced resistance oscillations and spike present different response to an increasing in-plane magnetic field. Resistance oscillations are shifted to higher perpendicular magnetic field (B), when the in-plane is increased. Yet, the spike approximately keeps the same position. Then, the authors suggest that both effect are ruled by different physical mechanisms.

Other strong resistance spikes in radiation-induced R_{xx} oscillations experiments were previously obtained around the cyclotron resonance $w \approx w_c$[17] for higher frequencies and power and being explained by resonant heating of electrons. Off-resonance phenomena are always remarkable phenomena in all branches of Physics. They are counterintuitive with respect to the basic reso-

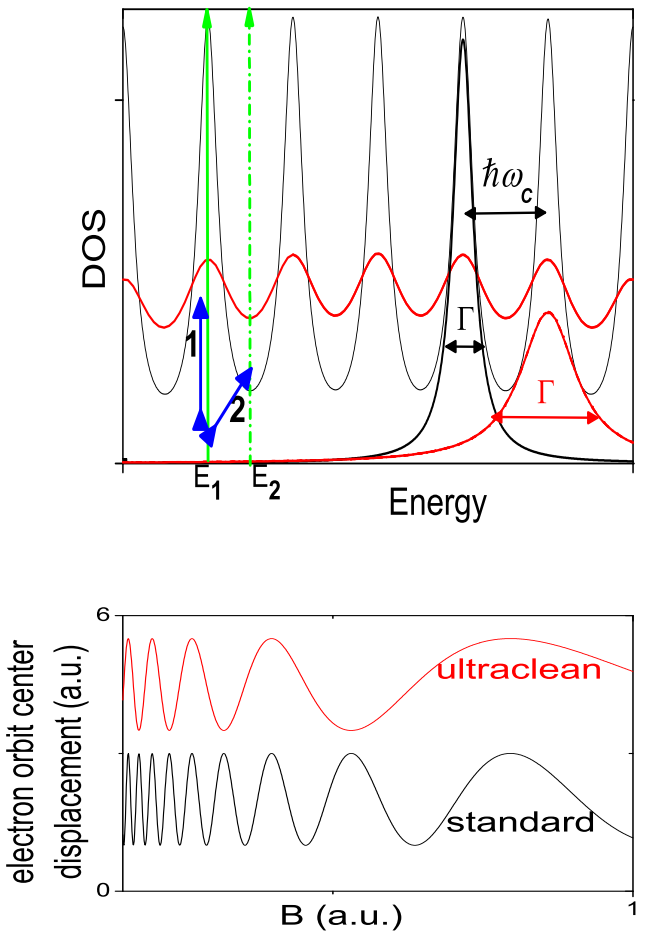

FIG. 1: Upper panel: schematic diagram showing the density of Landau states simulated by Lorentzian functions for wide and narrow Landau levels, where the width of the states is indicated by Γ. The arrow 1 corresponds to an elastic scattering process and the arrow 2 to an inelastic one. Lower panel: schematic diagram showing the radiation-driven electron orbit center displacement (two dimensional electron system) for ultraclean and standard samples. We observe that the first one is delayed regarding the latter as being driven by radiation of smaller frequency.

nance process, meaning a challenge to the available theory. Then, it would be important to fully understand these phenomena, not only from the basic standpoint but also from the application side. For instance, they could lead to the design and development of novel *ultrasensitive* photon detectors[27] in the microwave and terahertz bands, where the technology is not well-developed yet.

In this article, we theoretically study this radiation-induced R_{xx} spike applying the theory developed by the authors, *the radiation-driven electron orbits model*[4,5,28–30]. According to it, when a Hall bar is illuminated, the electron orbit centers perform a classical trajectory consisting in a harmonic displacement along the direction of the current at the w frequency. This motion is damped by the interaction of electrons with the lattice ions and with the consequent emission of acoustic phonons. Thus, the 2DES moves periodically at the radiation frequency altering dramatically the scattering conditions and giving rise eventually to R_{xx} oscillations and ZRS. We extend this model to a ultraclean sample, obtaining that all the scattering conditions are modified. Mainly because the LL, which in principle are broadened by scattering, become very narrow in this kind of samples. This implies an increasing number of states at the center of the LL sharing a similar energy. In between LL, it happens the opposite, the density of states decreases dramatically (see upper panel of Fig.1). Therefore, the elastic scattering rate, due to charged impurities, increases, meanwhile the inelastic one (phonon emission damping) decreases. Thus, the elastic scattering time (inverse of elastic scattering rate) decreases reaching a limiting value of half of the time of a standard sample. This specific value is related with the LL degeneracy. For the irradiated electrons, half of the scattering time is physically equivalent as being driven by radiation of frequency $w/2$. Accordingly, the cyclotron resonance is shifted to a new B-position around $w \approx 2w_c$. On the other hand, the inelastic scattering decreases and the emission of acoustic phonons is less efficient producing a *bottleneck effect* which prevents from releasing the absorbed energy to the lattice. Finally the corresponding amplitude abruptly increases giving rise to a strong resistance spike.

We also present a microscopical theoretical approach to the dependence of the LL width on the magnetic field for the regime of ultraclean samples. We apply this approach in the framework of the general theory of the radiation-driven electronic orbits model. We find that this dependence is very important to explain the experimental shift found in the resistance oscillations with respect to the magnetic field for this kind of samples[24]. We study also very recent results on the influence of an in-plane magnetic field on the spike and the corresponding connection with the resistance oscillations. We consider that the main effect of adding this parallel magnetic field is to increase the disorder perceived by the electrons in the sample. Within our model and among the different sources of scattering, inelastic scattering of electrons by interaction with acoustic phonons (emission) is the most directly affected. The basic result is a progressive damping of the spike and the whole radiation resistance response. This is observed in experiments[26]. The total scattering rate reflects also this increasing disorder which broadens the LL; now the LL width depends on both the perpendicular and in-plane magnetic fields. As feedback effect, this will eventually affect the charged impurity scattering rate. This feedback and the LL degeneracy cut-off value explain the different behavior of the spike and resistance oscillations with the in-plane magnetic field. Initially, all spike-related phenomena were tried to be explained[24] as unique events with an origin different from radiation-

induced R_{xx} oscillations. Yet, in this article we consider that the resistance spike and everything related with it, are the outcome of an extreme scenario of the radiation-induced oscillations in ultraclean samples and therefore, sharing the same physics.

II. THEORETICAL MODEL

A. Summary of the radiation-driven electron orbit model

The *radiation-driven electron orbits model*, was developed to explain the R_{xx} response of an irradiated 2DEG at low magnetic field. We first obtain an exact expression of the electronic wave function. Then, the total hamiltonian H can be written as[4]:

$$\begin{aligned} H &= \frac{P_x^2}{2m^*} + \frac{1}{2}m^* w_c^2 (x-X)^2 - eE_{dc}X + \\ &+ \frac{1}{2}m^* \frac{E_{dc}^2}{B^2} - eE_0 \cos wt(x-X) - \\ &- eE_0 \cos wtX \\ &= H_1 - eE_0 \cos wtX \end{aligned} \tag{1}$$

X is the center of the orbit for the electron spiral motion:

$$X = \frac{\hbar k_y}{eB} - \frac{eE_{dc}}{m^* w_c^2} \tag{2}$$

E_0 the intensity for the MW field and E_{dc} is the DC electric field in the x direction. H_1 is the hamiltonian corresponding to a forced harmonic oscillator whose orbit is centered at X. H_1 can be solved exactly[29,30], and using this result allows an exact solution for the electronic wave function[4]:

$$\Psi(x,t) = \phi_n(x - X - x_{cl}(t), t) exp\left[i\frac{m^*}{\hbar}\frac{dx_{cl}(t)}{dt}x + \frac{i}{\hbar}\int_0^t L dt' \right] \sum_{m=-\infty}^{\infty} J_m \left[\frac{eE_0}{\hbar}\left(\frac{1}{w} + \frac{w}{\sqrt{(w_c^2 - w^2)^2 + \gamma^4}} \right) \right] e^{imwt} \tag{3}$$

and the main result that we want to point out is that $\Psi_N(x,t) \propto \phi_n(x - X - x_{cl}(t), t)$ where ϕ_n is the solution for the Schrödinger equation of the unforced quantum harmonic oscillator. J_m are Bessel functions and L is a classical Lagrangian of an electron in the presence of magnetic field. $x_{cl}(t)$ is the classical solution of a forced and damped harmonic oscillator:

$$\begin{aligned} x_{cl} &= \frac{eE_o}{m^*\sqrt{(w_c^2 - w^2)^2 + \gamma^4}} \cos wt \\ &= A \cos wt \end{aligned} \tag{4}$$

where E_0 is the MW electric field. γ is a damping factor for the electronic interaction with the lattice ions giving rise to emission of acoustic phonons. Then, the obtained wave function is the same as the one of the standard quantum harmonic oscillator where the center is displaced by $x_{cl}(t)$. This implies that the electron orbit centers oscillate harmonically at w. This $radiation-driven$ behavior will affect dramatically the charged impurity scattering and eventually the conductivity.

Next, we calculate the scattering suffered by the electrons due to charged impurities (elastic) applying time dependent first order perturbation theory. Thus, we calculate the scattering rate[4,31,32] between two *oscillating* Landau states (LS), the initial, n, and the final, m:

$$W_{n,m} = \lim_{\alpha \to 0} \frac{d}{dt} \left| \frac{1}{i\hbar} \int_{-\infty}^{t'} < \Psi_m(x,t)|V_s|\Psi_n(x,t) > e^{\alpha t} dt \right|^2 \tag{5}$$

where V_s is the scattering potential for charged impurities[33],

$$V_s = \sum_q \frac{e^2}{2S\epsilon(q+q_0)} \cdot e^{i\vec{q}\cdot\vec{r}} \tag{6}$$

S being the surface of the sample, ϵ the GaAs dielectric constant, and q_0 is the Thomas-Fermi screening constant[33,34]. After some algebra we arrive at an intermediate expression for the charged impurities scattering rate:

$$\begin{aligned} W_{m,n} &= \frac{2\pi}{\hbar} | < \phi_m|V_s|\phi_n > |^2 \\ &\times \frac{2eB}{h} S \sum_{m=0}^{\infty} \frac{1}{\pi} \left[\frac{\Gamma}{(E_n - E_m)^2 + \Gamma^2} \right] \end{aligned} \tag{7}$$

Γ is the LL width and the last part of the expression represents the density of final Landau states, ρ_m, in the

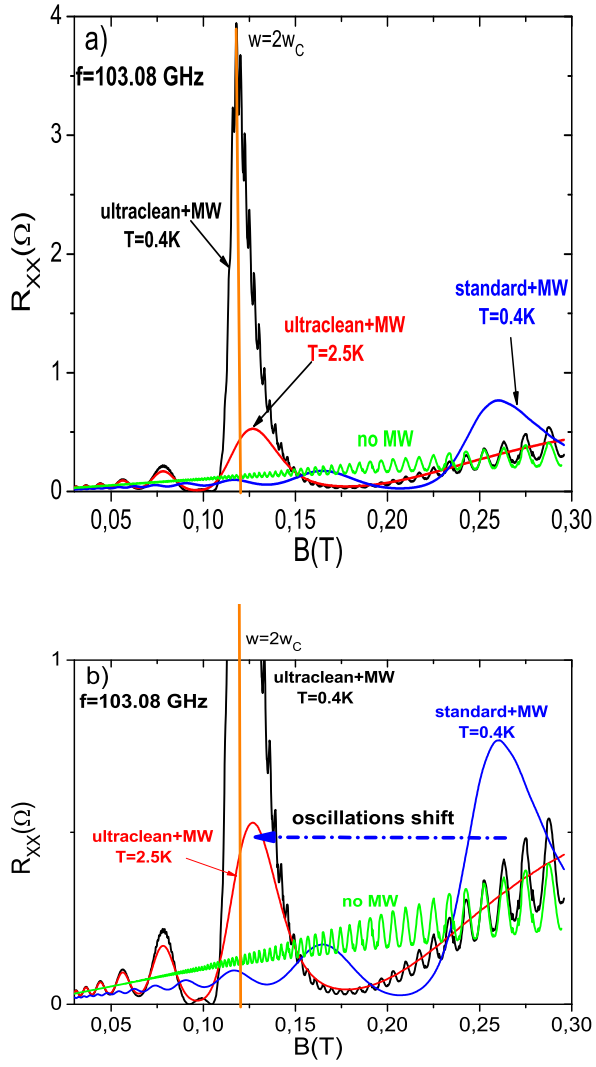

FIG. 2: a) Calculated irradiated magnetoresistance vs static magnetic field for a radiation frequency of $f = 103.08GHz$, different samples (standard and ultraclean) and temperatures. For ultraclean sample and a temperature of, $T = 0.4K$, we observe a intense spike at $w \approx 2w_c$. Yet, for higher temperature, $T \simeq 2.5K$, the spike vanishes. For a standard sample and low temperature, we obtain a curve with the usual radiation-induced resistance oscillations and zero resistance states but the spike does not show up. b) Blown-up of upper panel for lower magnetoresistance values. We observe that in ultraclean samples, radiation-induced oscillations are shifted to lower magnetic field positions, compared to standard sample case.

elastic scattering jump,

$$\rho_m = \frac{2eB}{h} S \sum_{m=0}^{\infty} \frac{1}{\pi} \frac{\Gamma}{(E_n - E_m)^2 + \Gamma^2} \tag{8}$$

E_n and E_m are the corresponding LL energies for the

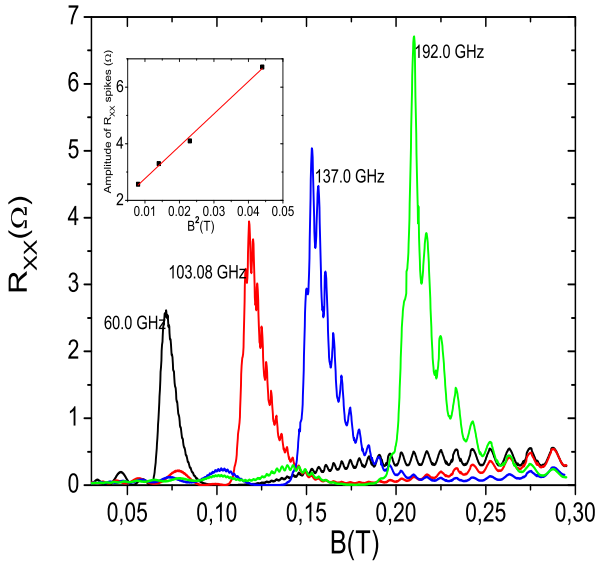

FIG. 3: Calculated irradiated magnetoresistance vs magnetic field for radiation frequencies $f = 60.0, 103.08, 137.0$ and 192 GHz. For each frequency we obtain a spike at $w \approx 2w_c$. The spike amplitude increases with the radiation frequency, and with the magnetic field as B^2. This dependence can be shown in the inset, where we present the amplitude of the spike vs the square of the magnetic field.

initial and final states respectively.

Once we know the scattering rate, we consider that when an electron undergoes a scattering process jumping from the initial state to the final one, it advances an average effective distance[4,28,32], ΔX^{rad}, given by

$$\Delta X^{rad} = \Delta X^0 + A \cos w\tau \tag{9}$$

where ΔX^0 is the effective distance advanced when there is no radiation field present. Then, following Ridley[32] we can obtain the expression for the longitudinal conductivity σ_{xx} according to the expression,

$$\sigma_{xx} \propto \int dE \frac{\Delta X^{rad}}{\tau_{uclean}} \tag{10}$$

being E the energy. Then, we get to the final expression which reads,

$$\sigma_{xx} = \frac{e^7 m^{*2} B n_i S}{\pi \epsilon^2 \hbar^6 q_0} \left[\Delta X^0 + A\cos w\langle\tau\rangle\right]^2 \left[1 + 2e^{\frac{-\pi\Gamma}{\hbar w_c}} + e^{\frac{-\pi\Gamma}{\hbar w_c}} \frac{X_S}{\sinh X_S}\left(\cos\frac{2\pi E_F}{\hbar w_c}\right)\right] \quad (11)$$

where n_i is the impurities density and $X_S = \frac{2\pi^2 k_B T}{\hbar w_c}$. To obtain R_{xx} we use the relation $R_{xx} = \frac{\sigma_{xx}}{\sigma_{xx}^2+\sigma_{xy}^2} \simeq \frac{\sigma_{xx}}{\sigma_{xy}^2}$, where $\sigma_{xy} \simeq \frac{n_i e}{B}$ and $\sigma_{xx} \ll \sigma_{xy}$. Therefore, we reach an expression for R_{xx} :

$$R_{xx} \propto \frac{eE_o}{m^*\sqrt{(w_c^2 - w^2)^2 + \gamma^4}} \cos w\tau \quad (12)$$

The radiation power, P, can be related with A through the well-known formula that gives radiation intensity I (power divided by surface) in terms of the radiation electric field E_0: $I = \frac{1}{2}c\epsilon_0 E_0^2$, where c is the speed of light in vacuum and ϵ_0 is the permittivity in vacuum. If we want to express only the power in terms of the radiation electric field we have to take into account the sample surface. In the particular case of GaAs we can readily obtain:

$$P = \frac{1}{2} c_{GaAs}\epsilon\epsilon_0 E_0^2 S \quad (13)$$

where c_{GaAs} is the speed of light in GaAs and ϵ is the GaAs dielectric constant. Accordingly,

$$E_0 \propto \sqrt{P} \quad (14)$$

Then, substituting in the expression of A, we obtain that R_{xx} varies with P following an square root law:

$$R_{xx} \propto \frac{e\sqrt{P}}{m^*\sqrt{(w_c^2 - \frac{w}{2}^2)^2 + \gamma^4}} \cos\frac{w}{2}\tau \quad (15)$$

Thus, we expect that the R_{xx} response will grow according to the square root of P, i.e., following a sublinear dependence which is finally reflected in the amplitude, $A \propto P^{0.5}$.

B. Far off-resonance position of the giant resistance spike

The precise shape of broadened LL in real systems (with disorder) remains, even currently, controversial. Usual assumptions are Gaussian[35–37], Lorentzian[38–41] and semielliptic[33], being the two first, the most commonly used. For instance, some published experimental results[42,43] indicate that they could be equally described or explained assuming either a Lorentzian or Gaussian profiles. More recently, other works related with radiation-induced R_{xx} oscillations and ZRS, have used Lorentzian shapes for LL in the corresponding theoretical models[24,44] In our case, dealing with ultraclean samples (very narrow LL), and low B and T, there is no much theoretical or experimental information about the real profile of the broadened Landau states. We have to consider that the samples used in the experiments[24,25] with extremely high mobilities have been very recently obtained. Then, we are facing a completely brand new scenario requiring more theoretical and experimental work. Therefore, as a first approach and following T. Ihn[45], we have assumed for the broadened density of Landau states a Lorentzian function being the width independent of the LL index.

If we rewrite eq. (8) considering that $E_m = \hbar w_c(m + \frac{1}{2})$,

$$\rho_m = \frac{2eB}{h} S \sum_{m=0}^{\infty} \frac{1}{\pi} \frac{\Gamma}{(E_n - \hbar w_c(m+\frac{1}{2}))^2 + \Gamma^2} \quad (16)$$

Now, this last expression can be further developed if we apply the Poison sum rules[45],

$$\sum_{m=0}^{\infty} f(m+\frac{1}{2}) = \int_0^{\infty} f(x)dx + 2\sum_{s=1}^{\infty}(-1)^s \int_0^{\infty} f(x)\cos(2\pi x s)dx \quad (17)$$

and then, we can reach for ρ_m,

$$\rho_m = \frac{m^*}{\pi\hbar^2}\left\{1 + 2\sum_{s=1}^{\infty}(-1)^s \cos\left[\frac{2\pi s E_n}{\hbar w_c}\right] exp\left[-\frac{\pi\Gamma s}{\hbar w_c}\right]\right\} \quad (18)$$

that with $E_n = \hbar w_c(n + \frac{1}{2})$ we finally obtain,

$$\rho_m = \frac{m^*}{\pi\hbar^2}\left\{1 + 2\sum_{s=1}^{\infty} exp\left[-\frac{\pi\Gamma s}{\hbar w_c}\right]\right\} \quad (19)$$

Normally in this calculations if the exponent is not very small it is enough to consider the first term $s = 1$. Yet, since we are dealing with high mobility samples and very small Γ the latter approximation can not be applied. Then if the total sum is carried out we obtain[46]:

$$\sum_{s=1}^{\infty} exp\left[-\frac{\pi\Gamma s}{\hbar w_c}\right] = \frac{exp\left[-\frac{\pi\Gamma}{\hbar w_c}\right]}{1 - exp\left[-\frac{\pi\Gamma}{\hbar w_c}\right]} \tag{20}$$

that translated into the final density of states,

$$\rho_m = \frac{m^*}{\pi\hbar^2}\left\{1 + 2\frac{exp\left[-\frac{\pi\Gamma}{\hbar w_c}\right]}{1 - exp\left[-\frac{\pi\Gamma}{\hbar w_c}\right]}\right\} = \frac{m^*}{\pi\hbar^2}\left\{\frac{1 + exp\left[-\frac{\pi\Gamma}{\hbar w_c}\right]}{1 - exp\left[-\frac{\pi\Gamma}{\hbar w_c}\right]}\right\} \tag{21}$$

Substituting this result in eq. (7), we arrive at the final expression for the charged impurities scattering rate which reads:

$$W_{m,n} = W_0\left(\frac{1 + exp\left[\frac{-\pi\Gamma}{\hbar w_c}\right]}{1 - exp\left[\frac{-\pi\Gamma}{\hbar w_c}\right]}\right) \tag{22}$$

where W_0[47] represents the charged impurities scattering rate for a *standard* mobility sample which is recovered for wide Γ,

$$W_0 = \frac{e^5 B m^* n_i S}{\hbar^4 \epsilon^2 q_0^2} \tag{23}$$

As we said above, for ultraclean samples Γ is very small and for experimental magnetic fields[24,25], it turns out that $\Gamma << \hbar w_c$. Then, if B increases, the exponent $\frac{-\pi\Gamma}{\hbar w_c}$ decreases making $W_{m,n}$ continuously to increase. However, there exists a cut-off defined by the LL degeneracy:

$$LLdegen. = \frac{2eB}{h} \tag{24}$$

In a regime of narrow LL the density of states ρ_m can be approximated considering that in an elastic scattering, such as the one caused by charged impurities, most processes take place at the center of the LL, sharing approximately the same energy (see Fig.1 upper panel) and then $E_m \simeq E_n$. This implies that,

$$\frac{2eB}{h}\frac{1}{\pi}\frac{\Gamma}{(E_m - E_n)^2 + \Gamma^2} \to \frac{2eB}{h}\frac{1}{\pi\Gamma} \tag{25}$$

In this regime of narrow Γ, in an interval energy of $\hbar w_c$ we must have, in average, a number of states given by the LL degeneracy and therefore:

$$\frac{2eB}{h}\frac{1}{\pi\Gamma} \times \hbar w_c \to \frac{2eB}{h} \tag{26}$$

This is only fulfilled if,

$$\frac{\hbar w_c}{\pi\Gamma} \to 1 \tag{27}$$

which is a remarkable result because translated into the expression of eq. (22) we obtain:

$$\frac{\hbar w_c}{\pi\Gamma} \to 1 \Rightarrow \left[\frac{1 + e^{\frac{-\pi\Gamma}{\hbar w_c}}}{1 - e^{\frac{-\pi\Gamma}{\hbar w_c}}}\right] \to 2 \Rightarrow W_{m,n} \simeq 2 \times W_0 \tag{28}$$

Then, the charged impurities scattering rate increases with B till a cut-off value of twice the corresponding of a standard sample. In terms of charged impurities scattering time,

$$\tau_{uclean} = \frac{1}{2}\tau \tag{29}$$

where $\tau = 1/W_0$ is the time of a standard sample and τ_{uclean} corresponds to a ultraclean one. Accordingly, the ultraclean scattering time, $\tau_{uclean} = \frac{1}{W_{mn}}$ turns out to be twice shorter than the standard and then, the scattering event is twice faster.

Within the framework of our theory[4], this implies that during the time τ_{uclean} and compared to the standard for the same B, the ultraclean 2DES appears to be displaced by radiation a smaller distance. In other words, in terms of scattering, the *ultraclean* harmonic motion (electron orbit center displacement) is perceived as delayed regarding the *standard*, as if electrons were driven by radiation of smaller frequency (see Fig. 1 lower panel), more precisely, of half frequency. Then, the radiation electric field, E_w, is perceived as,

$$E_w = E_0 \cos \frac{w}{2} t \tag{30}$$

by the ultraclean 2DES. The conclusion is that in ultraclean samples, during scattering, electrons "$feel$" radiation with half of the real frequency. Applying next the theory[4], we reach an expression for R_{xx} in the ultraclean case:

$$R_{xx} \propto \frac{eE_o}{m^* \sqrt{(w_c^2 - (\frac{w}{2})^2)^2 + \gamma^4}} \cos \frac{w}{2} \tau \tag{31}$$

According to it, now the resonance in R_{xx} will take place at $w \approx 2w_c$, as experimentally obtained[24,25].

C. Intensity of the resistance spike

The intensity of the R_{xx} spike will depend on the relative value of the frequency term, $(w_c^2 - (\frac{w}{2})^2)$, and the damping parameter γ in the denominator of the latter R_{xx} expression. When γ leads the denominator the spike is smeared out. Yet, in situations where γ is smaller than the frequency term, the resonance effect will be more visible and the spike will show up. As we explained above, the parameter γ represents the interaction of electrons with the lattice ions, damping the electronic orbits motion and releasing radiation energy in form of acoustic phonons. Therefore, γ is given by[33]:

$$\gamma = \frac{1}{\tau_{ac}} \propto T \times \frac{2eB}{h} \sum_{m=0}^{\infty} \frac{1}{\pi} \left[\frac{\Gamma}{(E_n - \hbar w_{ac} - E_m)^2 + \Gamma^2} \right] \tag{32}$$

where w_{ac} is the frequency of acoustic phonons for experimental parameters[24,25] and the last term represents the density of final Landau states. Following similar steps as before we obtain the expression:

$$\gamma = \frac{2\Xi^2 m^* k_B T}{v_s^2 \rho \pi \hbar^3 < z >} \times \left\{ 1 + 2 \sum_{s=1}^{\infty} exp \left[-\frac{\pi \Gamma s}{\hbar w_c} \right] \cos \left[\frac{2\pi s \hbar w_{ac}}{\hbar w_c} \right] \right\} \tag{33}$$

where Ξ is the acoustic deformation potential, ρ the mass density, k_B the Boltzman constant, T the temperature, vs the sound velocity and $< z >$ is the effective layer thickness. When the total sum inside brackets is carried out we obtain[46],

$$\sum_{s=1}^{\infty} exp \left[-\frac{\pi \Gamma s}{\hbar w_c} \right] \cos \left[\frac{2\pi s \hbar w_{ac}}{\hbar w_c} \right] = = \frac{e^{\left[-\frac{\pi \Gamma}{\hbar w_c} \right]} \left\{ \cos \left[\frac{2\pi \hbar w_{ac}}{\hbar w_c} \right] - e^{\left[-\frac{\pi \Gamma}{\hbar w_c} \right]} \right\}}{1 - 2e^{\left[-\frac{\pi \Gamma}{\hbar w_c} \right]} \cos \left[\frac{2\pi \hbar w_{ac}}{\hbar w_c} \right] + e^{\left[-\frac{2\pi \Gamma}{\hbar w_c} \right]}} \tag{34}$$

Then, substituting in γ we finally obtain,

$$\gamma = \frac{2\Xi^2 m^* k_B T}{v_s^2 \rho \pi \hbar^3 < z >} \left\{ \frac{1 - e^{\left[-\frac{2\pi \Gamma}{\hbar w_c} \right]}}{1 - 2e^{\left[-\frac{\pi \Gamma}{\hbar w_c} \right]} \cos \left[\frac{2\pi \hbar w_{ac}}{\hbar w_c} \right] + e^{\left[-\frac{2\pi \Gamma}{\hbar w_c} \right]}} \right\} \tag{35}$$

In order to have an approximate but more compact version of eq. (27) we can consider average values for the cyclotron energy and for the acoustic phonon energy in the case of experimental parameters. Thus, for the magnetic fields swept in the experiments we can take in average that the cyclotron energy is $\hbar w_c \sim 2 \times 10^{-4}$ meV, and the phonon acoustic energy is, $\hbar w_{ac} \sim 1 \times 10^{-4}$ meV.

Then, for those values the cosine term,

$$\cos\left[\frac{2\pi\hbar w_{ac}}{\hbar w_c}\right] \sim -1 \tag{36}$$

that gives an expression for the damping parameter which reads

$$\gamma = \frac{2\Xi^2 m^* k_B T}{v_s^2 \rho\pi\hbar^3 < z >}\left(\frac{1-e^{\frac{-\pi\Gamma}{\hbar w_c}}}{1+e^{\frac{-\pi\Gamma}{\hbar w_c}}}\right) \tag{37}$$

According to this last expression, for increasing B the term inside brackets decreases and as a result, the parameter γ will get smaller, making increasingly difficult the damping by acoustic phonon emission and the release of the absorbed energy to the lattice. Therefore, we have a *bottleneck effect* for the emission of acoustic phonons. Now it is possible to reach a situation where $(w_c^2 - (\frac{w}{2})^2)^2 \gtrsim \gamma^4$ making visible a resonance effect and, therefore, giving rise to a strong resonance peak at $w \approx 2w_c$. For GaAs and standard experimental parameters[2,3], we obtain that $\gamma \simeq 7 - 10 \times 10^{11} s^{-1}$ and that in a ultra-clean regime[24,25] it decreases till $\sim 3.5 \times 10^{11}$. This fixes a lower cut-off value for the radiation frequency where the resistance spike could be observed. According to our calculations this would be around $f = w/2\pi \approx 40 - 45GHz$. Experiments have also pointed out that at lower frequencies is much more difficult to observe resistance spikes.

D. Variation of Γ with the magnetic field for ultraclean samples

One important issue which plays a key role in the model presented above is the dependence of Γ on the magnetic field. Previous experimental and theoretical works[35–41] report that for lower B (but higher than 1 T), Γ varies with the magnetic field as $\sim \sqrt{B}$. Yet, for increasing B, Γ becomes independent. For our brand new scenario of extremely high mobility samples at very low B, (~ 0.1 T), and very low temperature, (~ 0.4 K), there is no much information, experimental or theoretical, about the actual dependence of Γ on B. Therefore, and as a first approach, we have developed a simple microscopical description, based in scattering parameters, of this dependence which starts from previous analytical expressions[33,35,37,42,45,48]. Thus, following T. Ihn[45], we begin with the expression which relates Γ and B,

$$\Gamma(B) = \sqrt{\frac{\hbar^2 w_c}{2\pi\tau_0}} = \sqrt{\frac{\hbar^2 e}{2\pi m^* \tau_0}}\sqrt{B} \tag{38}$$

where τ_0 is the zero magnetic field quantum scattering lifetime.

For the experimental spikes[24,25], the magnetic field used is very low, around $B \sim 0.1T$. Then, for this regime we can assume that the variation of Γ with B is closer to a straight line than to a square root and proceed to linearize the latter expression. Thus, we expand the square root by a Taylor series around $B = 0.1$ T, till the first derivative term. Then, we can write,

$$\Gamma(B) = \Gamma(0.1) + (B - 0.1)\Gamma'(0.1) \tag{39}$$

and finally obtain the expression which gives the dependence of Γ on B for very low B

$$\Gamma(B) \propto \frac{1}{2\sqrt{0.1}}\sqrt{\frac{\hbar^2 e}{2\pi m^* \tau_0}} B^p \tag{40}$$

where $p \to 1$. p is a phenomenologically introduced parameter which takes into account that the dependence of Γ on B does not follow strictly a straight line but it is close to it. In our case we have assigned $p \sim 0.90$. This expression implies that, for extremely high mobility samples and very low B, the Landau states broaden almost linearly with the magnetic field affecting all scattering processes such as elastic impurity scattering and inelastic phonon scattering. This dependence of Γ on B has been used throughout the above theoretical model on spikes.

E. Influence of an in-plane magnetic field

The effect of an in-plane magnetic field, ($B_\parallel$), on the radiation-induced resistance oscillations was already studied and published[49], and experimental results showed that the main effect was a progressive damping of the whole resistance response as $B_\parallel$ increased. Subsequent theoretical results[50], confirmed and explained the surprising damping in the framework of the radiation-driven electrons orbits model. Accordingly and as we said above, in an irradiated 2DES in the presence of a perpendicular B, electronic orbits are forced to move back and forth, oscillating harmonically at the frequency of radiation and with an amplitude proportional to the radiation electric field. In their radiation-driven motion, electrons interact with the lattice ions being damped and producing acoustic phonons. The presence of $B_\parallel$ imposes an extra harmonically oscillating motion in the z-direction enlarging the electrons trajectory in their orbits. This would increase the interactions with the lattice making the damping process more intense and reducing the amplitude of the orbits oscillations. Therefore, the effect of the presence of $B_\parallel$ is to increase the disorder in the sample from the electrons perspective.

The Hamiltonian for electrons confined in a 2D system (x-y plane) by a potential $V(z)$ and subjected to a total magnetic field $B_T = (B_x, 0, B)$, ($B_{||} = B_x$) is given considering the previous hamiltonian of eq. (1) by:

$$H = H_1 - eE_0 \cos wtX + H_z \tag{41}$$

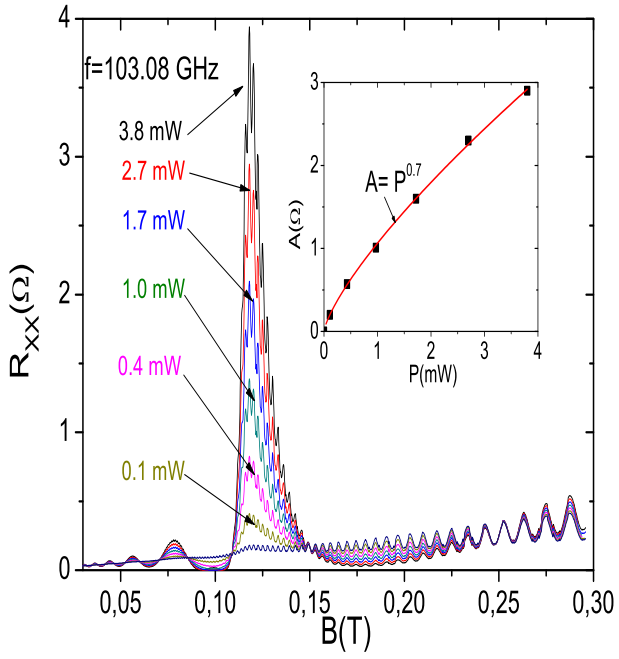

FIG. 4: Calculated irradiated magnetoresistance vs static magnetic field for different radiation power (P) and a frequency $f = 103.08GHz$. P varies from 3.8 mW to 0.1 mW, including $P = 2.7$, 1.7, 1.0 and 0.4 mW. For decreasing P, the radiation-induced magnetoresistance response decreases as well, and for $P = 0.1mW$ we obtain a response close to darkness. In the inset we present the spike amplitude vs P. We fit the data obtaining a sublinear P-dependence, $R_{xx} \propto P^{\alpha}$ where α is close to 0.5.

If we consider a parabolic potential for V_z,

$$V(z) = \frac{1}{2} m^* w_0^2 z^2 \tag{42}$$

the Hamiltonian H_z can be written as:

$$\begin{aligned} H_z &= \frac{P_z^2}{2m^*} + \frac{1}{2} m^* (w_x^2 + w_0^2) z^2 \\ &= \frac{P_z^2}{2m^*} + \frac{1}{2} m^* \Omega^2 z^2 \end{aligned} \tag{43}$$

We have used the the Landau gauge for B_x: $\overrightarrow{A_{B_x}} = (0, -zB_x, 0)$, and

$$w_x = \frac{eB_x}{m^*} \tag{44}$$

The use of a parabolic potential for V_z allows that the corresponding time-dependent Schrodinger equation of H can be readily solved. We obtain the wave functions of two harmonic oscillators, one in the x direction and the other in the z-direction:

$$\Psi_T(x, z, t) \propto \phi_N \left[(x - X - x_{cl}(t)), t \right] \phi(z) \tag{45}$$

In a semiclassical approach the electron is subjected simultaneously to two independent harmonic motions with a trajectory depicted in Fig. 9: As we have indicated above, the presence of in-plane B alters the electron trajectory in its orbit increasing the frequency and the number of oscillations in the z-direction. Now the frequency of the z-oscillating motion is $\Omega > w_0$. This makes longer the electron trajectory increasing the total orbit length and eventually the damping. This increase in the orbit length is proportionally equivalent to the increase in the number of oscillations in the z-direction. Thus, we introduce the ratio of frequencies after and before connecting B_x as a correction factor for the damping factor γ. The final damping parameter γ_f is:

$$\begin{aligned} \gamma_f &= \gamma \times \frac{\Omega}{w_0} = \gamma \times \sqrt{1 + \left(\frac{w_x}{w_0} \right)^2} \\ &= \gamma \times \sqrt{1 + \left(\frac{eB_x z_0^2}{\hbar} \right)^2} \end{aligned} \tag{46}$$

where z_0 is the effective length of the electron wave function when we consider a parabolic potential for the z-confinement[33,34],

$$z_0 = \sqrt{\frac{\hbar}{m^* w_0}} \tag{47}$$

The expression of γ_f shows that one of the main results of the presence of B_x is an increase in the damping parameter due to the interaction with lattice ions. Therefore, the whole resistance response to radiation, (spike and oscillations) will be increasingly damped. The second important effect is reflected in the total quantum scattering rate $1/\tau_0$. According to the Matthiessen rule the total scattering rate can be expressed as the sum of the different individual scattering sources, $\frac{1}{\tau_0} = \sum_i \frac{1}{\tau_i}$ and obviously one of them is the acoustic phonon scattering rate. The increase in the phonon scattering rate ($\gamma = 1/\tau_{ac}$) due to B_x will eventually affect the total scattering rate that will increase as well, making it B_x-dependent, $\frac{1}{\tau_0(B_x)}$. Considering the Matthiessen rule and the ratio of frequencies $\frac{\Omega}{w_0}$ affecting γ, we can readily obtain the expression,

$$\begin{aligned} \frac{1}{\tau_0(B_x)} &= \frac{1}{\tau_0} + \gamma \left[\frac{\Omega}{w_0} - 1 \right] \\ &= \frac{1}{\tau_0} + \gamma \left[\sqrt{1 + \left(\frac{eB_x z_0^2}{\hbar} \right)^2} - 1 \right] \end{aligned} \tag{48}$$

And now eq. (40) can be rewritten taking into account the last expression,

$$\Gamma(B, B_x) \simeq \frac{1}{2\sqrt{0.1}} \sqrt{\frac{\hbar^2 e}{2\pi m^* \tau_0(B_x)}} B^p \qquad (49)$$

Now Γ depends on both magnetic fields the perpendicular B and the in-plane B_x,

III. RESULTS

In Fig.1 in the upper panel, we present a schematic diagram showing the density of Landau states for wider and narrow Γ, (standard and ultraclean samples respectively). Therefore, we can observe the two different regimes; for a standard sample where $\hbar w_c < \Gamma$ and for a ultraclean one where $\hbar w_c > \Gamma$. The broadened Landau states have been simulated by Lorentzian functions. The arrow 1 corresponds to an elastic scattering process (remote charged impurity scattering) and the arrow 2 to an inelastic one (acoustic phonon scattering). In the lower panel of Fig. 1, we present the radiation-driven electron orbit displacement for ultraclean and standard samples. We observe that the first one is delayed regarding the latter as being driven by radiation of smaller frequency.

In Fig. 2a, we present calculated irradiated R_{xx} vs static magnetic field for a radiation frequency of $f = 103.08GHz$. The presented results correspond to standard and ultraclean samples and high and low temperatures. For the ultraclean sample and $T = 0.4K$, we obtain a strong spike at $w \approx 2w_c$ as in experiments[24,25]. Increasing temperature for the same sample, $(T \simeq 2.5K)$ the spike vanishes but the radiation-induced oscillations still remain but with lower intensity, as expected. Finally, for a standard sample, we obtain the usual radiation-induced R_{xx} oscillations and ZRS. In Fig. 2b we present a blown up of the lower values of R_{xx} of the upper panel. Thus, we can contrast the curve of the ultraclean sample with the standard, observing a shift of the R_{xx} oscillations to lower magnetic fields.

In our calculations we have used a quantum lifetime at zero magnetic field $\tau_0 \sim 2 \times 10^{-11}$ s,[24,25,51] for the ultraclean R_{xx} curve, which gives us, according to eq. (32), a LL width of $\Gamma \sim 5. \times 10^{-4} B^p$ eV. For the standard curve, we have used a shorter quantum lifetime,[44,52–54] $\tau_0 \sim 10^{-12}$ s, giving a broader Γ, $\Gamma \simeq 25.10^{-4} B^p$ eV. The quantum life time defines the quality of the sample; the longer this time, the higher the quality and narrower Γ. Smaller Γ, according to eq. (22), will give us a longer impurity scattering time. Then, the perceived radiation frequency will be smaller, shifting the R_{xx} oscillations to lower B as observed in ultraclean samples. On the other hand, with a shorter quantum life time (low quality samples or standard), Γ is large and the term inside brackets in eq. (22) tends to 1. Thus, we recover the usual positions for radiation-driven R_{xx} oscillations[17].

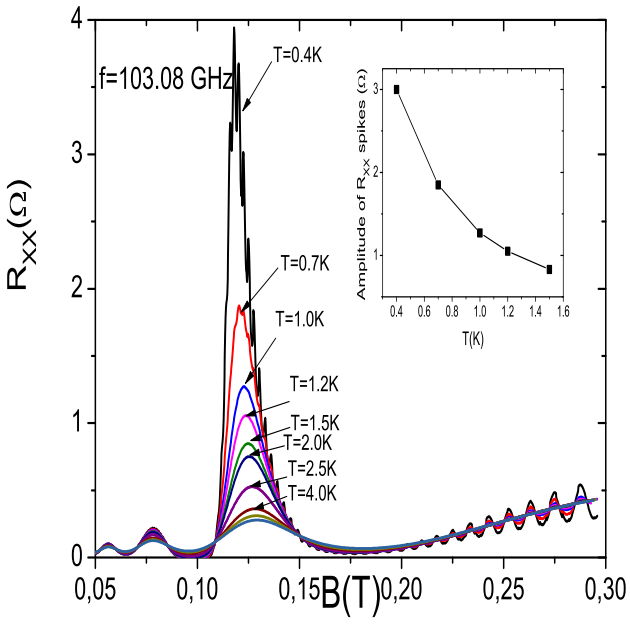

FIG. 5: Calculated irradiated magnetoresistance vs magnetoresistance for different temperatures and a frequency $f = 103.08GHz$. Temperature varies from 0.4 k to 4.0 K. We observe a clear decrease of the spike and R_{xx} oscillations for increasing T. The T-dependence is explained with the damping parameter γ which represents the interaction of electrons with acoustic phonons. In the inset we present the amplitude of the spike vs T. We fit the data obtaining a relation $R_{xx} \propto T^{-2}$ (hyperbole), as expected from the model.

In Fig. 3 we present calculated irradiated R_{xx} vs magnetic field for different radiation frequencies $f = 60.0$, 103.08, 137.0 and 192 GHz. For all cases we obtain a clear spike at $w \approx 2w_c$. We observe that the spike amplitude increases with the frequency and as a result with the magnetic field. This is because of the presence of the frequency term, $(w_c^2 - \frac{w}{2}^2)^2$ in the denominator of the R_{xx} expression, and then, the higher w, the higher the magnetic field where the resonance takes place. In the inset of the figure we observe that the amplitude of the corresponding spike grows with the magnetic field following a B^2 law. This expected from our model[47] because according to it, the radiation-dependent part of the R_{xx} depends on the magnetic field as B^2. Therefore, we predict for the amplitude of the *"$w \approx 2w_c$ spike"*, a square law dependence on B^2 that would need to be experimentally confirmed. The experiments that discovered the R_{xx} spike showed that the amplitude increases with the frequency. Yet, they do not present any law or fit showing the increase rate of the spike amplitude with B.

In Fig. 4 we present calculated irradiated R_{xx} vs mag-

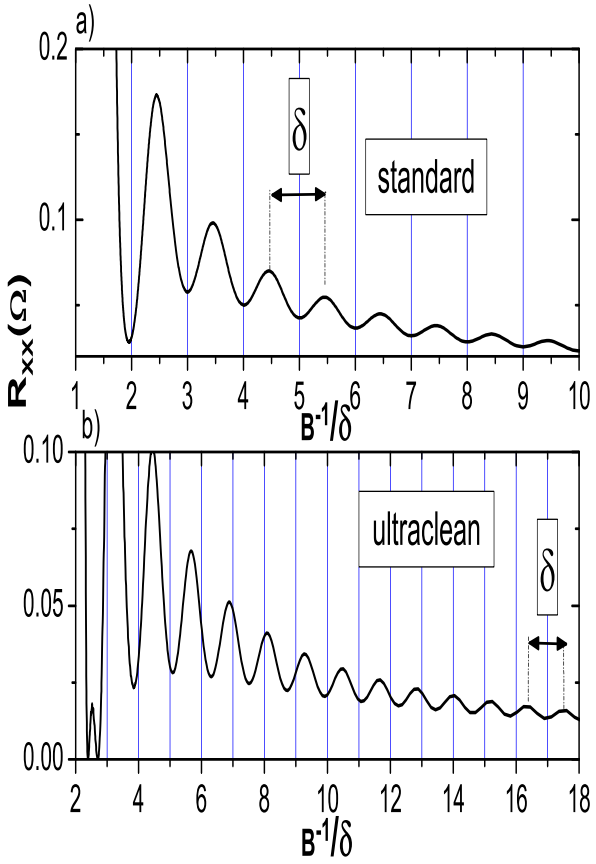

FIG. 6: Normalized B^{-1} plots of calculated data on radiation induced resistance oscillations of Fig. 2 for standard sample (6a) and for ultraclean (6b). δ's are the oscillatory periods in B^{-1} for each case.

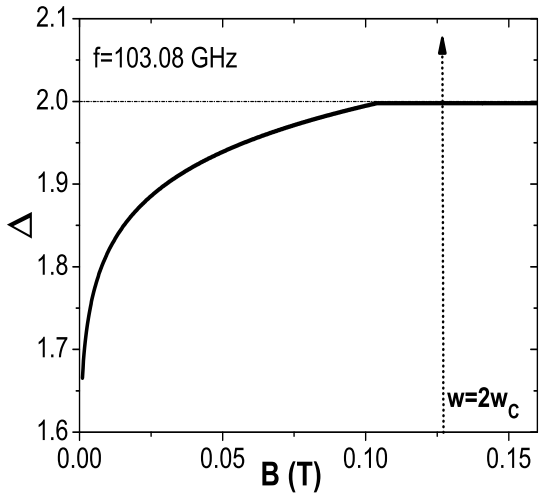

FIG. 7: Calculated values for Δ versus B. For $B \simeq 0$ the term $\Delta \to 1$ because the absolute value of the exponents is very large. Then, as B increases the exponents decrease and Δ increases till the cut-off value of 2. This makes the impurity scattering rate continuously to increase with B from $\Delta \simeq 1$ to $\Delta \simeq 2$, or impurity scattering time to decrease. This effect is perceived by the electrons as if radiation had a decreasing frequency. Eventually, the back and forth motion of electrons in their orbits is performed at a decreasing frequency too.

netic field for different radiation power (P) and frequency $f = 103.08GHz$. P varies from 3.8 mW to 0.1 mW, including P = 2.7, 1.7, 1.0 and 0.4 mW. Decreasing P, the radiation-induced R_{xx} response, (spike and oscillations), decreases as well, and for $P = 0.1mW$ we obtain nearly the darkness result. In the inset we present the amplitude of the R_{xx} spike vs P. We fit the data obtaining a sublinear P-dependence, $R_{xx} \propto P^{\alpha}$ where α is close to 0.5, as expected, and explained in terms of our model: $E_0 \propto \sqrt{P} \Rightarrow R_{xx} \propto \sqrt{P}$ and in agreement with experimental[21] and theoretical[55] results.

In Fig. 5 we present calculated irradiated magnetoresistance vs magnetic field and frequency $f = 103.08GHz$, for differente temperatures (T). T varies from 0.4 to 4.0 K. We observe a clear decrease of the spike for increasing T, till it is smeared out. The T-dependence, according to the model, is explained with the damping parameter γ. γ is linear with T[4,28], and $R_{xx} \propto \gamma^{-2}$. Thus, an increasing T means an increasing γ and smaller both spike and R_{xx}

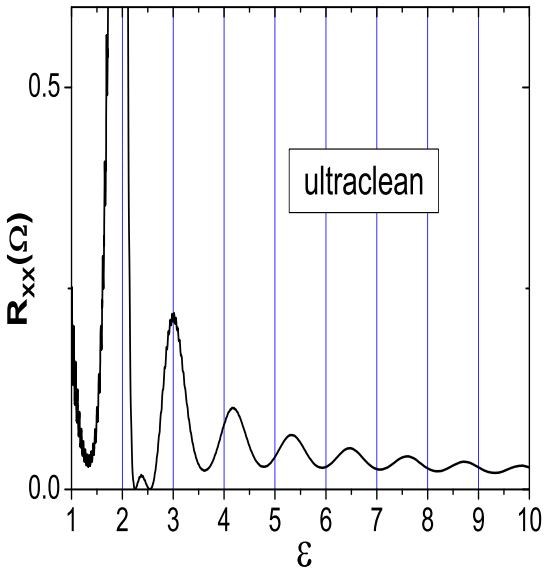

FIG. 8: Calculated irradiated R_{xx} vs ε for a frequency of $f = 103.08$ GHz. We observe a qualitatively similar shift as in experiment[24]. Yet, quantitatively speaking the calculated shift is larger than the obtained in the experiment[24].

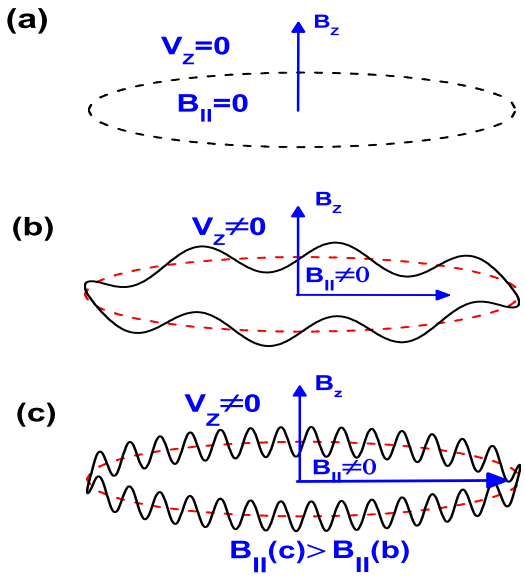

FIG. 9: Schematic diagrams showing the semiclassical description of electron trajectories in 2D systems. In the three of them there is present a perpendicular magnetic field B_z that explains the circular trajectories. a) 2DES ($x-y$ plane) and B_z. b) 2DES, B_z, a parabolic potential V_z and an in-plane magnetic field $B_{||}$. c) Same as b) but the intensity of $B_{||}$ is bigger.

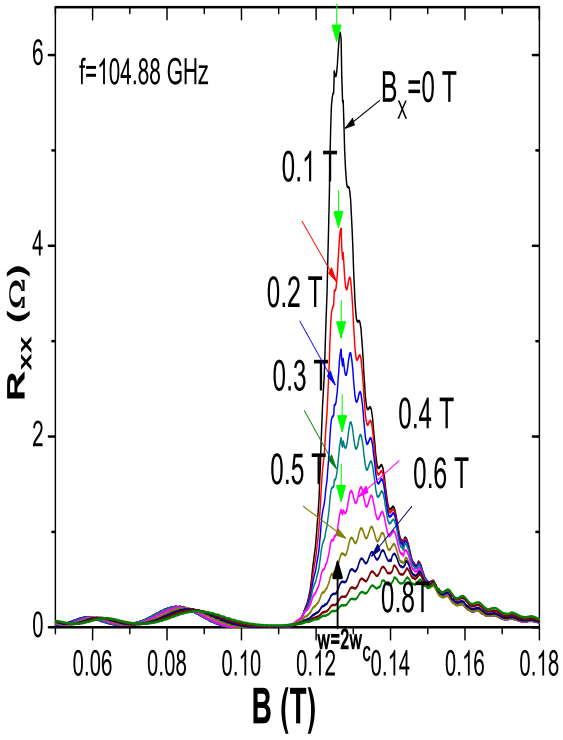

FIG. 10: Calculated irradiated R_{xx} versus B for a radiation frequency of $f = 104.88$ GHz and for different values of the in-plane magnetic field B_x. B_x goes from 0T till 0.8T in intervals of 0.1T. We first observe a progressive damping of the resistance spike and resistance oscillations. For approximately $B_x = 0.6$ T the spike has been completely removed. We observe as well that starting from $B_x = 0.5$ and for larger B_x the main R_{xx} associated with the spike shifts to higher B. However, we observe that from $B_x = 0$ T till $B_x = 5$ T, the R_{xx} spike remains approximately in its position, although its intensity is progressively smaller. The green arrows highlight this effect.

oscillations. When the damping is strong enough (higher T) all R_{xx} response collapses giving a final result close to darkness. The inset shows the relation $R_{xx} \propto T^{-2}$ (hyperbole), as expected from the model.

In Fig. 6 we present normalized B^{-1} plots of calculated data of radiation induced R_{xx} oscillations of Fig. 2, ($f = 103.08GHz$), for standard (6a) and ultraclean (6b) samples. δ's are the oscillatory periods in B^{-1} for each case. In the standard case we observe a nearly perfect periodic curve with respect to B^{-1}, as experimentally observed[2]. This is explained with the linear dependence on B of the charged impurity scattering rate (see eqs. (22) and (23)) when the brackets term tends to 1 (standard samples). This implies that the charged impurity scattering time depends inversely on B, giving the periodic curve of Fig. 6a ($R_{xx} \propto A\cos w\tau$). In the ultraclean case, we observe an oscillatory behavior of R_{xx} versus B^{-1} but it is not perfectly periodic. Instead, we observe a shift of the R_{xx} oscillations regarding the vertical lines defined by the period. Peaks and valleys are increasingly shifted. As B increases, the distance between subsequent peaks (or valleys) increases.

The origin of this effect is in the exponents of eq. (22) which depend on B. The dependence on B of the charged impurity scattering rate comes not only from the linear term of W_0 of that equation, but also from the exponentials in the brackets term what we call Δ,

$$\Delta = \left(\frac{1 + exp\left[\frac{-\pi\Gamma}{\hbar w_c}\right]}{1 - exp\left[\frac{-\pi\Gamma}{\hbar w_c}\right]} \right) \qquad (50)$$

The variation of Δ with B is presented in Fig. 7. For B close to 0, $\Delta \to 1$ because the absolute value of the exponents is very large. Then, as B increases the exponents decrease and Δ continuously increases till the cut-off value of 2. This makes the charged impurity scattering rate continuously to increase with B from $\Delta \simeq 1$ to $\Delta \simeq 2$, (or impurity scattering time to decrease). This effect is perceived by the electrons as if radiation had a decreasing frequency. Eventually all of this is reflected in the obtained R_{xx} where the distance between R_{xx} peaks

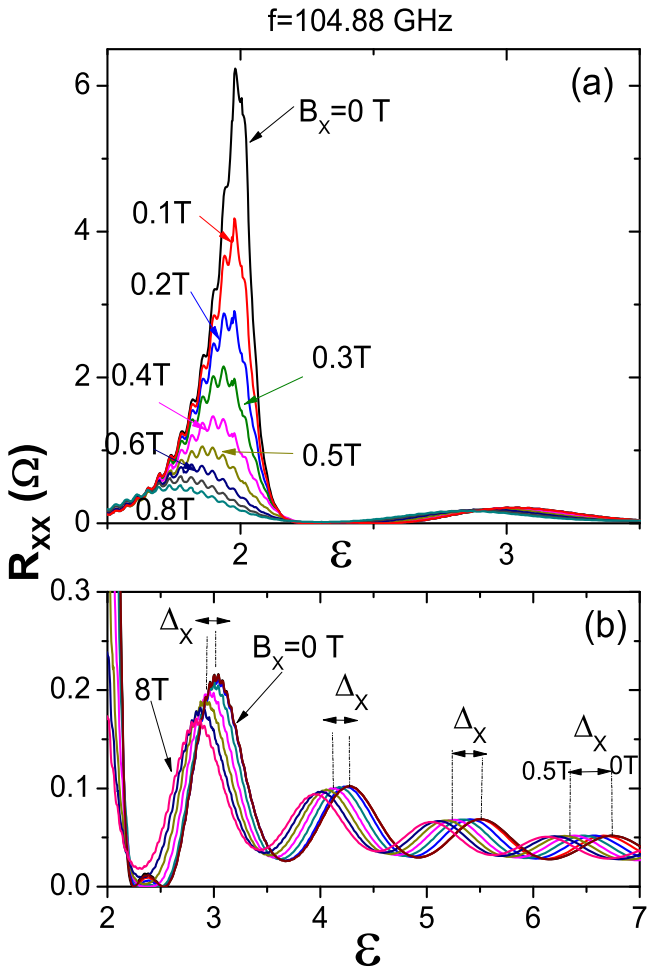

FIG. 11: Calculated irradiated R_{xx} vs ε for a frequency of $f = 103.08$ GHz. In a) ε goes from 1.5 to 3.5. As in Fig. 10 we observe the spike keeping the same position till $B_x = 5$ T. Starting from $B_x = 6$, the main resistance peak associated with the spike shifts to higher B as B_x increases. In b) ε goes from 2 to 7. We observe the shift, also to higher B, of the other resistance peaks. The shift is represented by Δ_x. Yet, in apparent contradiction, the corresponding spike stands still for the same B_x values as observed in a).

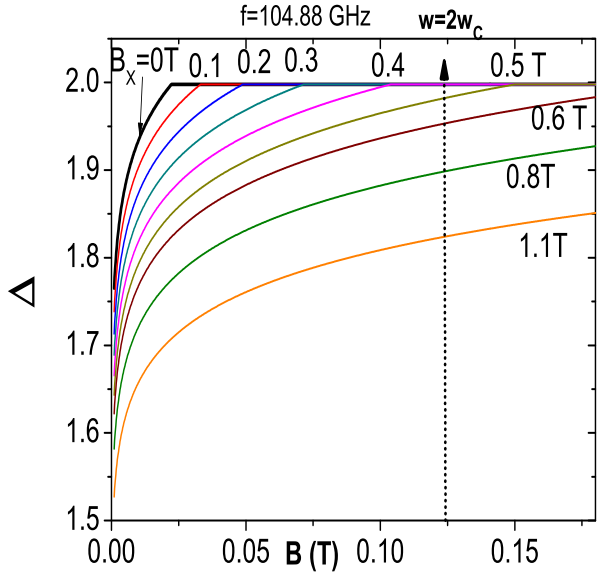

FIG. 12: Calculated values of Δ term versus B for same values of B_x as in Fig. 10, and $B_x = 1.1$ T. The interpretation is similar to Fig. 7. The presence of an increasing B_x, gives rise to larger Γ which as a result makes Δ to decrease. Then, the impurity scattering time decreases continuously being reflected in the perceived radiation frequency which decreases too. The final outcome is that R_{xx} oscillations shift to higher B as B_x increases. This is a general behavior for all values of B_x. We can see in the figure that from $B_x = 0$ T till $B_x = 5$ the threshold of $\Delta \simeq 2$ is achieved in the sweeping B before the resonance condition of $w = 2w_c$ or around it. Then, when reaching this condition, the resonance effect can take place and an intense R_{xx} spike will rise in the same position for all of them,

(or valleys) gets larger. This is what explains the obtained shift in Fig. 6b.

From the experimental standpoint a similar shift can be found in Fig. 1b of reference [24]. In this Fig. it is represented the difference between resistivity under radiation minus dark resistivity versus the parameter $\varepsilon = \frac{w}{w_c}$ and obtained an oscillation shift of 0.25 of the period. According to the experimental results[24], the shift is increasingly larger for decreasing B. To contrast our calculated results on this shift with experiment we present in Fig. 8 calculated R_{xx} vs ε. We obtain a qualitative agreement because we obtain a similar variation of the oscillations shift with B. Yet, quantitatively speaking we obtain a larger value, reaching 0.5 of the period. The reason for this quantitative discrepancy could be explained by the simple microscopical model used to describe the dependence of Γ on B for ultraclean samples. On the other hand, the model is able to explain the existence of the shift, its variation with B and the connection with the resistance spike.

In Fig. 9, we present schematic diagrams showing the semiclassical description of electron trajectories in 2DES (x-y plane), under a perpendicular magnetic field in the z-direction ($B_z = B$). We present three cases. In a) we have the basic situation of only a 2DES and B_z. In the case b) we add to a) a parabolic potential V_z and an in-plane magnetic field $B_\parallel$. And finally in the case c) we have the same as b) but the intensity of $B_\parallel$ is larger. In a semiclassical approach the electron dynamics under simultaneously these two magnetic fields can be interpreted as being subjected to two independent harmonic motions with trajectories depicted in Fig. 9. When one

considers only B_z, the electron performs a circular movement in the $x-y$ plane, (see Fig. 9a). In Fig. 9b, we add a parabolic potential in the z direction and we introduce $B_{\|}$, then the electron trajectory is circular in the plane and at the same time is oscillating in z. In Fig. 9c $B_{||}$ increases and the number of oscillations in z direction increases too.

In Fig. 10 we present calculated irradiated R_{xx} versus B for a radiation frequency of $f = 104.88$ GHz and for different values of the in-plane magnetic field B_x. B_x goes from 0 T till 0.8 T in intervals of 0.1 T. We first observe a progressive damping of the R_{xx} spike and oscillations. For approximately $B_x = 0.6$ T the spike has been completely removed. We observe as well that for $B_x > 0.5$, the main R_{xx} peak associated with the spike, shifts to higher B. As we have previously explained, the main effect of B_x is an increase of disorder in the sample. In our approach this is reflected in a stronger interaction of electrons with the lattices ions giving rise to a more intense emission of acoustic phonons. Then, the absorbed radiation energy can be more efficiently released and the resistance response tends to progressively collapse. This is similar to the effect of an increasing lattice temperature as previously presented (see Fig. 5). Remarkably we observe that from $B_x = 0$ T till $B_x = 5$ T, the R_{xx} spike remains approximately in its position, (see green arrows in Fig. 10), although its intensity is progressively smaller.

In Fig. 11a, we present similar information as in Fig. 10 but this time versus ε. In Fig. 11b, we present a blown up of 11a for ε values from 2 to 7. We observe that meanwhile the spike does not move when we sweep B_x from $B_x = 0$ T till $B_x = 5$ T, the corresponding resistance oscillations present a clear shift to higher B. One could think in principle that such different B_x responses could indicate different physical origin. However following our theory, they are totally connected. And the explanation has to do, as before, with the variation of Γ with the magnetic field. The explanation can be obtained from Fig.12.

In Fig. 12 we present the Δ term versus B for same values of B_x as in Fig. 10, and adding $B_x = 1.1$ T. In principle, the interpretation is similar to Fig. 7. Now the presence of an increasing B_x, gives rise to larger Γ which as a result makes Δ to decrease. Then, the impurity scattering time decreases continuously being reflected in the perceived radiation frequency which decreases too. The final outcome is that R_{xx} oscillations shift to higher B as B_x increases. The effect is similar as having increasingly dirtier samples. This is a general behavior for all values of B_x. The only difference is that for increasing B_x, Δ grows slower versus B. Yet, we can see in the figure that from $B_x = 0$ T till $B_x = 5$ the threshold of $\Delta \simeq 2$ is achieved in the sweeping B before the resonance condition of $w = 2w_c$ or around it. Then, when reaching this condition, the resonance effect can take place and an intense R_{xx} spike will rise in the same position for all of them, as experimentally obtained[26]. Therefore, we obtain some B_x values, ($B_x \leq 5$) where constant spike position coexist with a shift of R_{xx} oscillations to larger B. For the B_x values that reach $\Delta \simeq 2$ after the resonance condition, the spike apparently would rise at higher B but the intense damping effect done by B_x makes it to vanish and can not be observed any longer. However, the shift of R_{xx} oscillations still can be observed and an example is the shift of the main R_{xx} peak associated with the spike.

IV. CONCLUSIONS

In summary, we have theoretically studied the recently discovered intense radiation-induced magnetoresistance peak obtained in ultraclean 2DES. The most remarkable feature of such a peak is that it shows up at $w \approx 2w_c$ and with an amplitude of an order of magnitude larger than the standard radiation-induced magnetoresistance oscillations. We apply the radiation-driven electron orbits model and we calculate the charge impurity elastic scattering rate, which increases in ultraclean samples, to obtain the novel resonance peak position (far off resonance). We obtain the inelastic scattering rate by phonon damping, which decreases in ultraclean samples, showing that it is responsible of the large peak amplitude. We present a microscopical model to explain the dependence of the LL width (Γ) on the magnetic field for ultraclean samples. We find that this B-dependent variation of Γ is essential to explain the experimental shift found in the resistance oscillations. Accordingly, the shift and the resistance spike are physically connected.

We have studied also very recent results on the influence of an in-plane magnetic field on the spike. According to them radiation-driven resistance oscillations and spike offer different behavior when this magnetic field is increased, as if they had different physical origin. The same model allows us to explain such surprising results. We conclude that the role of the in-plane magnetic field is mainly to increase the disorder making the ultraclean sample to behave progressively as a dirtier sample and affecting the total scattering rate and the width of the LL. Now, the simultaneous dependence of this width on B and B_x explains the apparent contradiction. Another important physical effect observed in experiments[24] for the first time in ultraclean samples is an important decrease in the measured resistance for very low magnetic fields. This effect is obtained without radiation and is described in the experiments as a pronounced negative magnetoresistance. Yet, as the magnetic field increases, the usual values of standard magnetoresistance are recovered. This effect, closely related with the quality of the sample, is the main topic of a future work. Calculated results are in good agreement with experiments. These results are remarkable also from a technological standpoint. For instance in nanophotonics where they could lead to the design and development of *ultrasen-*

sitive photon detectors in the microwave and terahertz bands where the technology is not mature yet.

V. ACKNOWLEDGMENTS

This work is supported by the MCYT (Spain) under grant MAT2011-24331 and ITN Grant 234970 (EU).

VI. REFERENCES

[1] J. Iñarrea, G. Platero, Phys. Rew. B, **51**, 5244, (1995);Europhys. Lett. **34**, 43, (1996);Europhys Lett. **33**, 477, (1996); Europhys Lett. **40**, 417, (1997).

[2] R. G. Mani, J. H. Smet, K. von Klitzing, V. Narayanamurti, W. B. Johnson, and V. Umansky, Nature(London) **420**, 646 (2002); R. G. Mani, V. Narayanamurti, K. von Klitzing, J. H. Smet, W. B. Johnson, and V. Umansky, Phys. Rev. B**69**, 161306 (2004).

[3] M. A. Zudov, R. R. Du, L. N. Pfeiffer, and K. W. West, Phys.Rev. Lett. **90**, 046807 (2003).

[4] J. Iñarrea and G. Platero, Phys. Rev. Lett. **94** 016806, (2005); J. Iñarrea and G. Platero, Phys. Rev. B **72** 193414 (2005)

[5] J. Iñarrea and G. Platero, Appl. Phys. Lett., **89**, 052109, (2006);J. Iñarrea and G. Platero, Phys. Rev. B, **76**, 073311, (2007); J. Iñarrea, Appl. Phys. Lett. **90**, 172118, (2007)

[6] A.C. Durst, S. Sachdev, N. Read, S.M. Girvin, Phys. Rev. Lett.**91** 086803 (2003)

[7] C.Joas, J.Dietel and F. von Oppen, Phys. Rev. B **72**, 165323, (2005)

[8] X.L. Lei, S.Y. Liu, Phys. Rev. Lett.**91**, 226805 (2003)

[9] Ryzhii et al, Sov. Phys. Semicond. 20, 1299, (1986)

[10] P.H. Rivera and P.A. Schulz, Phys. Rev. B **70** 075314 (2004)

[11] Junren Shi and X.C. Xie, Phys. Rev. Lett. **91**, 086801 (2003)

[12] M.G. Vavilov et. al., Phys. Rev. B, **70**, 161306 (2004)

[13] R. G. Mani et al., Phys. Rev. Lett. **92**, 146801 (2004).

[14] R. G. Mani et al., Phys. Rev. B**69**, 193304 (2004).

[15] R. L. Willett, L. N. Pfeiffer, and K. W. West, Phys. Rev. Lett. **93**, 026804 (2004).

[16] R. G. Mani, Physica E (Amsterdam) **22**, 1 (2004);

[17] J. H. Smet et al., Phys. Rev. Lett. 95, 116804 (2005).

[18] Z. Q. Yuan et al., Phys. Rev. B **74**, 075313 (2006).

[19] D. Konstantinov and K. Kono, Phys. Rev. Lett. **103**, 266808 (2009)

[20] S. I. Dorozhkin, L. Pfeiffer, K. West K, K. von Klitzing, J.H. Smet, Nat. Phys., **7**, 336, (2011)

[21] R. G. Mani, C. Gerl, S. Schmult, W. Wegscheider, V. Umansky, Phys. Rev. B **81**, 125320 (2010)

[22] S. Wiedmann, G.M. Gusev, O.E. Raichev, A.K. Bakarov and J.C. Portal, Phys. Rev. Lett., **105**, 026804, (2010)

[23] I.A. Dimitriev, M.G. Vavilov, I.L. Aleiner, A.D. Mirlin, and D.G. Polyakov, Phys. Rev. B, **71**, 115316, (2005)

[24] Yanhua Dai, R.R. Du, L.N. Pfeiffer and K.W. West, Phys. Rev. Lett., **105**, 246802, (2010).

[25] A.T. Hatke, M.A. Zudov, L.N. Pfeiffer and K.W. West, Phys. Rev. B **83**, 121301(R), (2011).

[26] Yanhua Dai, Kristjan Stone, Ivan Knez, Chi Zang, R.R. Du, Changli Yang, L.N. Pfeiffer and K.W. West, Phys. Rev. B. **84**, 241303(R), (2011).

[27] R. G. Mani, Appl. Phys. Lett., **92**, 102107, (2008)

[28] J. Inarrea and G. Platero, Appl. Physl Lett. **89**, 172114, (2006);Appl. Physl Lett., **91**, 252112, (2007)

[29] E.H. Kerner, Can. J. Phys. **36**, 371 (1958) .

[30] K. Park, Phys. Rev. B **69** 201301(R) (2004).

[31] J. Iñarrea and G. Platero, Appl. Phys Lett. **93**, 062104, (2008);J. Iñarrea, Appl. Phys Lett. **92**, 192113,(2008)

[32] B.K. Ridley. Quantum Processes in Semiconductors, 4th ed. Oxford University Press, (1993).

[33] T. Ando, A. Fowler and F. Stern, Rev. Mod. Phys.,**54**,(1982).

[34] John H. Davies, The Physics of Low-dimensional Semiconductors, Cambridge University Press, (1997).

[35] P.T. Coleridge, P. Zawadzki and A. S. Sachrajda, Phys. Rev. B, **49**, 10798, (1994)

[36] M.E. Raikh and T.V. Shahbazyan, Phys. Rev. B, **47**, 1522, (1993)

[37] L. Wang and R.F. O'Connell, Phys. Rev. B, **37**, 3052, (1988)

[38] P.T. Coleridge, R. Stoner and R. Fletcher, Phys. Rev. B, **39**, 1120, (1989)

[39] M.A. Itskovsky, Phys. Rev. B, **64**, 024415, (2001)

[40] M. Dragosavac et. al., Semicond. Sci. Technol., **20**, 664, (2005)

[41] H. Fujioka, S. Katsumoto and Y. Iye, Jpn. J. Appl. Phys., **40**, 2073, (2001)

[42] A. Potts, et. al., J. Phys.: Condens. Matter, **8**, 5189, (1996)

[43] Y.M. Zhou et. al., Physica B, **407**, 116, (2012)

[44] S.A. Studenikin, M. Potemski, A. Sachrajada, M. Hilke, L.N. Pfeiffer and K.W. West, Phys. Rev. B, **71**, 245313, (2001)

[45] Thomas Ihn. Semconductor Nanostructures. Quantum States and Electronic Transport. 1st ed. Oxford University Press, (2010).

[46] I.S. Gradshteyn and I.M. Ryzhik, Tables of Integrals, Series and Products. 6th ed. Academic Press. (2000).

[47] J. Inarrea and G. Platero, Phys. Rev. B, **84**, 075313, (2011).

[48] V. Sayakanit, et. al., Phys. Rev. B, **38**, 1340, (1988).

[49] C.L. Yang, R.R. Du, L.N. Pfeiffer and K.W. West, Phys. Rev. B, **74**, 045315, (2006).

[50] J. Iñarrea and G. Platero, Phys. Rev. B,. **78**, 193310,(2008).

[51] A.D. Chepelianskii et. al., arXiv:11022314v1

[52] M. Cunkurtaran, et. al., Phys. stat. sol. (b), **207**, 139, (1998)

[53] S. Wiedmann et. al., Phys. Rev. B, **82**, 165333, (2010)

[54] G.M. Gusev, S. Wiedman, Phys. Rev. B, **83**, 0413006(R),

(2011)
[55] Jesus Inarrea, R.G. Mani and W. Wegscheider, Phys. Rev. B,**82** 205321 (2010)